Supplementary Information

Improved photodegradation of anionic dyes using a complex graphitic carbon nitride and iron-based metal-organic framework material

Huan V. Doan,[‡a,b] Hoa Thi Nguyen,[‡b] Valeska P. Ting,[c] Shaoliang Guan,[d,e] Jean-Charles Eloi,[a] Simon R. Hall[a] and Xuan Nui Pham[*b]

[a]*School of Chemistry, University of Bristol, Bristol BS8 1TS, United Kingdom*

[b]*Department of Chemical Engineering, Hanoi University of Mining and Geology, 18 Pho Vien, Duc Thang, Bac Tu Liem District, Hanoi, Vietnam*

[c]*Department of Mechanical Engineering, University of Bristol, Bristol BS8 1TR, United Kingdom*

[d]*School of Chemistry, Cardiff University, Cardiff CF10 3AT, United Kingdom*

[e]*HarwellXPS, Research Complex at Harwell, Rutherford Appleton Laboratory, Didcot OX11 0FA, United Kingdom*

[‡]Joint first authorship: both authors contributed equally to this work

[*]Corresponding author. Email address: phamxuannui@humg.edu.vn (XNP)

Contents

1. Materials

Chemical reagents used in this study including urea ($(NH_2)_2CO$), hydrogen peroxide (H_2O_2), hydroxyl sodium (NaOH), sulphuric acid (H_2SO_4), ethylene glycol (EG), dimethylformamide (DMF), iron(III) chloride hexahydrate ($FeCl_3.6H_2O$), Reactive Red 195 (RR 195) and Reactive Yellow 145 (RY 145) were supplied by Sigma-Aldrich and used as received without further purification. Polyethylene terephthalate (PET) water bottles were used as a source of plastic wastes for the preparation of terephthalic acid (TPA).

2. Characterisation techniques

The crystal structure of synthesized samples was determined by X-ray powder diffraction (XRD) patterns using a D8 ADVANCE (Cu $K\alpha_1$ copper radiation, λ=0.154 nm, 3^o min^{-1} scanning speed, Bruker). The Fourier Transform Infrared (FT-IR) spectra were measured using a FTIR Affinity-1S (Shimadzu). X-ray photoelectron spectroscopy (XPS) measurements were performed using a Kratos Axis SUPRA XPS fitted with a monochromated Al kα X-ray source

(1486.7 eV), a spherical sector analyser and 3 multichannel resistive plates, 128 channel delay line detectors. All data was recorded at 150W and a spot size of 700 x 300 µm. Survey scans were recorded at pass energy of 160 eV, and high-resolution scans recorded at pass energy of 20 eV. Electronic charge neutralization was achieved using a magnetic immersion lens. Filament current = 0.27 A, charge balance = 3.3 V, filament bias = 3.8 V. All sample data was recorded at a pressure below 10^{-8} Torr and a room temperature of 294 K. Data was analysed using CasaXPS v2.3.20PR1.0 and the spectra were calibrated with C1s peak at 284.8 eV.

Scanning electron microscope (SEM) samples were coated with 15nm high purity graphite (Q150TES from Quorum Technologies Ltd, UK) for elemental analysis and to prevent charging. The micrographs and energy dispersive X-ray spectroscopy (EDS) maps were taken on a JSM-IT300 (JEOL, Japan), operated at 15kV, at a working distance of 10 mm, together with an X-max 80mm^2 detector, run with Aztec software. Transmission electron micrographs were obtained from a JEM-2100F (JEOL, Japan) at 200kV, with the samples drop cast onto carbon (high purity)-coated copper grids. The Brunauer-Emmett-Teller (BET) specific surface area and pore size distribution were determined using N_2 adsorption-desorption at 77 K on a Micromeritics TriStar II Plus. All samples were degassed at 150 °C for 12 h prior to measurement. Surface areas were determined using a multipoint BET method using adsorption data in the relative pressure (P/P_o) range 0.05-0.3. Pore size distributions were determined using the Barrett–Joyner–Halenda (BJH) method.

UV-Vis diffuse reflectance (UV-Vis DRS) and photoluminescence (PL) spectra were recorded on UV-2600 spectrophotometer (Shimadzu) and Cary Eclipse fluorescence spectrophotometer (Varian), respectively. The optical bandgap energy of the samples was estimated by using the following Kubelka-Munk equation[1] as follows:

$$\alpha h\nu = \mathrm{A}(h\nu - E_g)^{n/2} \qquad (1)$$

where E_g is the bandgap energy, A is the absorption constant, h is Planck constant, α and ν represents the optical absorption coefficient and light frequency, respectively. n is determined by the transition modes of semiconductors (direct electronic transitions at n = 1).[2] α can be calculated from absorption constant A and thickness of the sample t using $\nu = 2.303A/t$. $h\nu$ can be calculated from wavelength using $h\nu$ = 1240/wavelength. Practically, the bandgap energies E_g of the samples were determined from a plot of $(\alpha h\nu)^{1/2}$ versus $h\nu$ (Kubelka-Munk plot, see Figure S2), by extrapolating the straight-line portion of the curves to zero absorption coefficient value.

The point of zero charge (*pzc*) of O-g-C_3N_4/MIL-53(Fe) was measured by a salt addition method.[3] Typically, 50 mg of each sample was dispersed in 50 ml KCl 0.1 M in six 100-ml glass Erlenmeyer flasks by magnetically stirring for 30 min. The initial pH values (pH_o) of the suspension were then adjusted to several values between 2 and 12 by adding 0.25 M HCl or NaOH solution, measured by a calibrated Hach pHC201 pH meter with accuracy = ±0.02. After shaking for 24 h in a revolving water bath to reach equilibrium, resulting pH values were measured and the difference between the initial and final pH values ($\Delta pH = pH - pH_o$) against the initial pH was plotted. The pH value where ΔpH was zero was taken as the *pzc*.

The degradation experiments of RR 195 and RY 145 were carried out under solar irradiation. The sunlight intensity in the lab was measured with a pyranometer, showing the average solar flux is 700 lx. The concentration of the supernatant was analysed using the Shimadzu UV-2450 UV visible spectrophotometer (the absorption peak positions for RR 195 and RY 145 are at 541 nm and 419 nm, respectively). The dyes degradation was calculated using the following equation.

$$Dye\ degradation\ (\%) = \frac{C_o - C}{C_o} \times 100\% \quad (2)$$

where C_o (ppm) is the initial concentration and C (ppm) is the calculated concentration of anionic dyes in the supernatant taken from the reaction after 1 - 5 h.

Trapping experiments were performed to indicate the active species involved in photodegradation of RR 195 and RY 145. ~40 µl of each 10^{-6} M scavenger (*i.e.* tert-butyl alcohol (TBA), potassium dichromate ($K_2Cr_2O_7$), ammonium oxalate monohydrate (AO) and 1.4-benzoquinone ($^{\cdot}O_2^-$)) was added in the dyes solution (50 ppm of RR 195 or RY 145) containing 50 mg of O-g-C_3N_4/MIL-53(Fe). The photodegradation, in which hydroxyl radicals ($^{\bullet}OH$), electrons ($\bar{e}$), holes (h^+) and superoxide radicals ($^{\bullet}O_2^-$) were trapped by the scavengers, was calculated as above.

3. Additional information and results

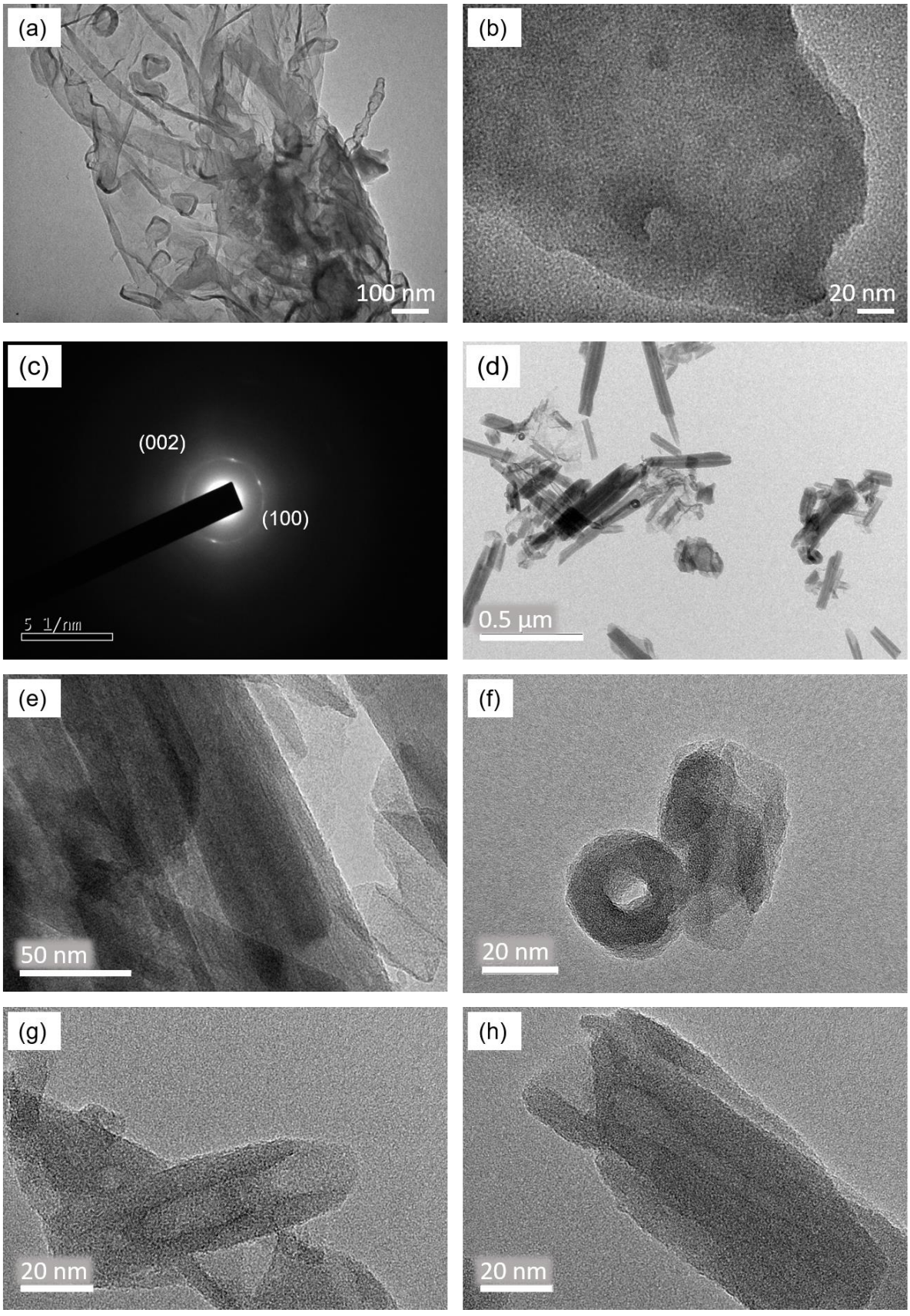

Figure S1. (a and b) TEM images of O-g-C_3N_4. (c) SAED spectra and (d-h) additional TEM images of O-g-C_3N_4/MIL-53(Fe) composite

Table S1. EDX elemental composition of O-g-C_3N_4/MIL-53(Fe) composite analysis)

Element	Weight (%)	Atomic (%)
C	38.34	50.96
O	26.65	26.59
Fe	20.39	5.83
N	14.62	16.62
Total	100.00	100.00

Table S2. BET specific surface (S_{BET}), pore volume (V_p) and pore size (D) of O-g-C_3N_4, MIL-53(Fe) and O-g-C_3N_4/MIL-53(Fe) composite

Samples	S_{BET} ($m^2\ g^{-1}$)	V_p ($cm^3\ g^{-1}$)	D (nm)[a]
O-g-C_3N_4	22.1	0.117	21.21/23.64
MIL-53(Fe)	20.4	0.052	10.27/11.80
O-g-C_3N_4/MIL-53(Fe)	28.6	0.136	19.13/23.75

[a]Pore diameters calculated from the adsorption/desorption branch of the isotherm using the Barrett–Joyner–Halenda (BJH) method.

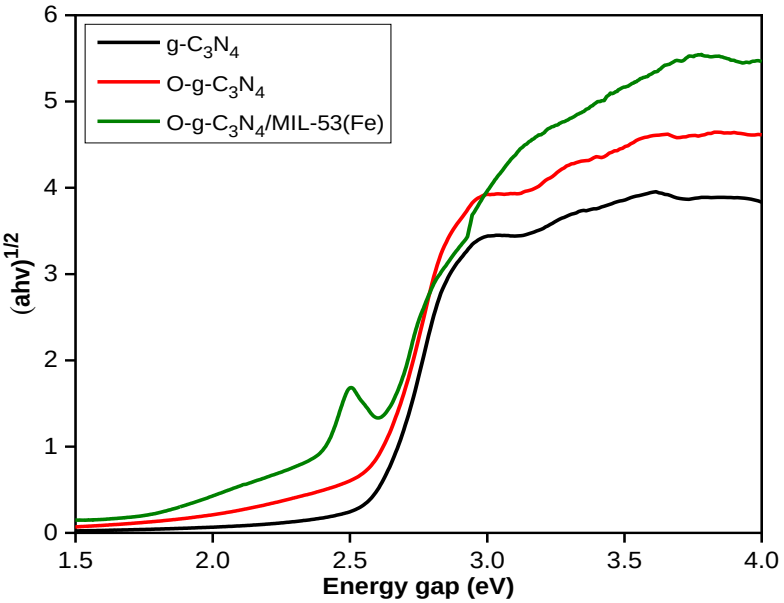

Figure S2. Kubelka-Munk plots of g-C_3N_4, O-g-C_3N_4, and O-g-C_3N_4/MIL-53(Fe) composite.

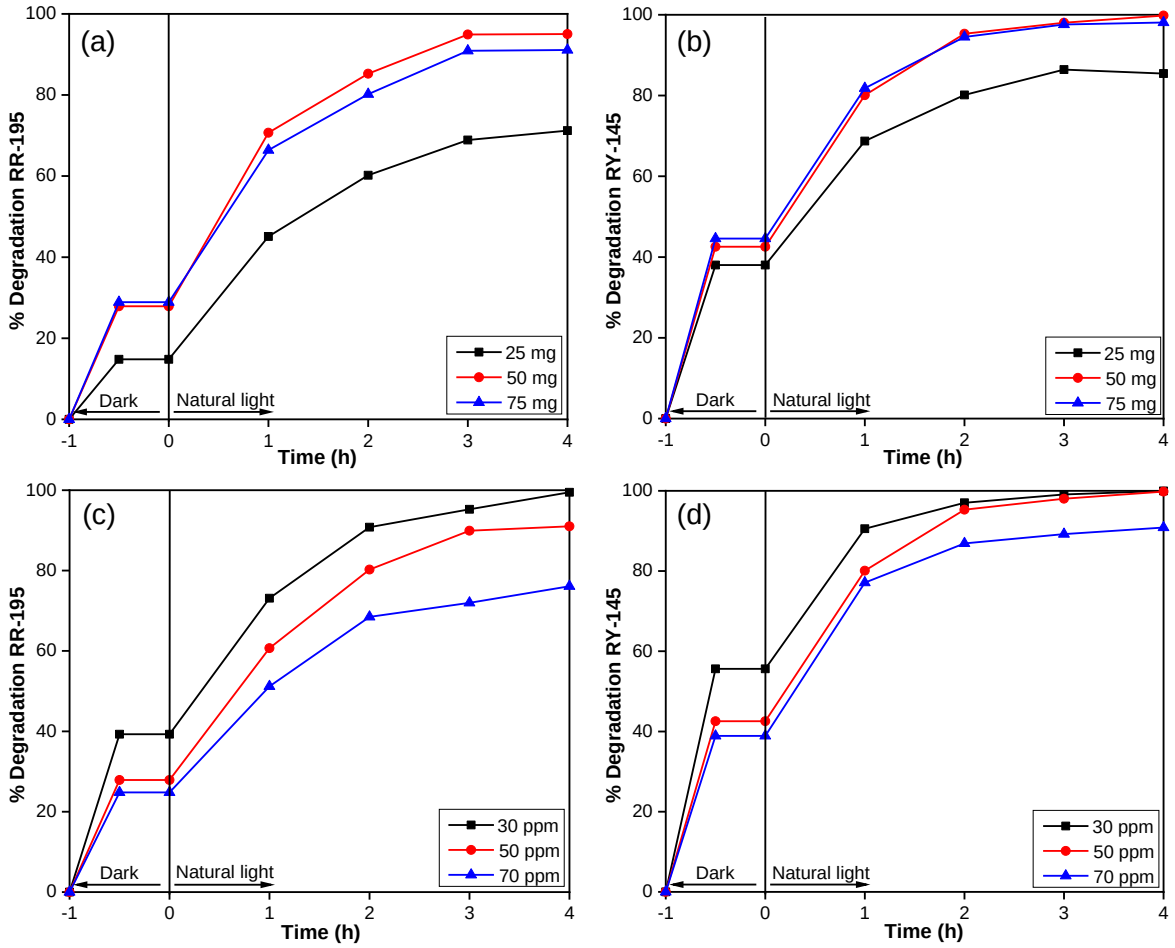

Figure S3. Photocatalytic degradation of (a) RR 195 and (b) RY 145 at the initial concentration of 50 ppm using different amounts of O-g-C_3N_4/MIL-53(Fe). Photocatalytic degradation of (c) RR 195 and (d) RY 145 at different initial concentrations using 50 mg of O-g-C_3N_4/MIL-53(Fe).

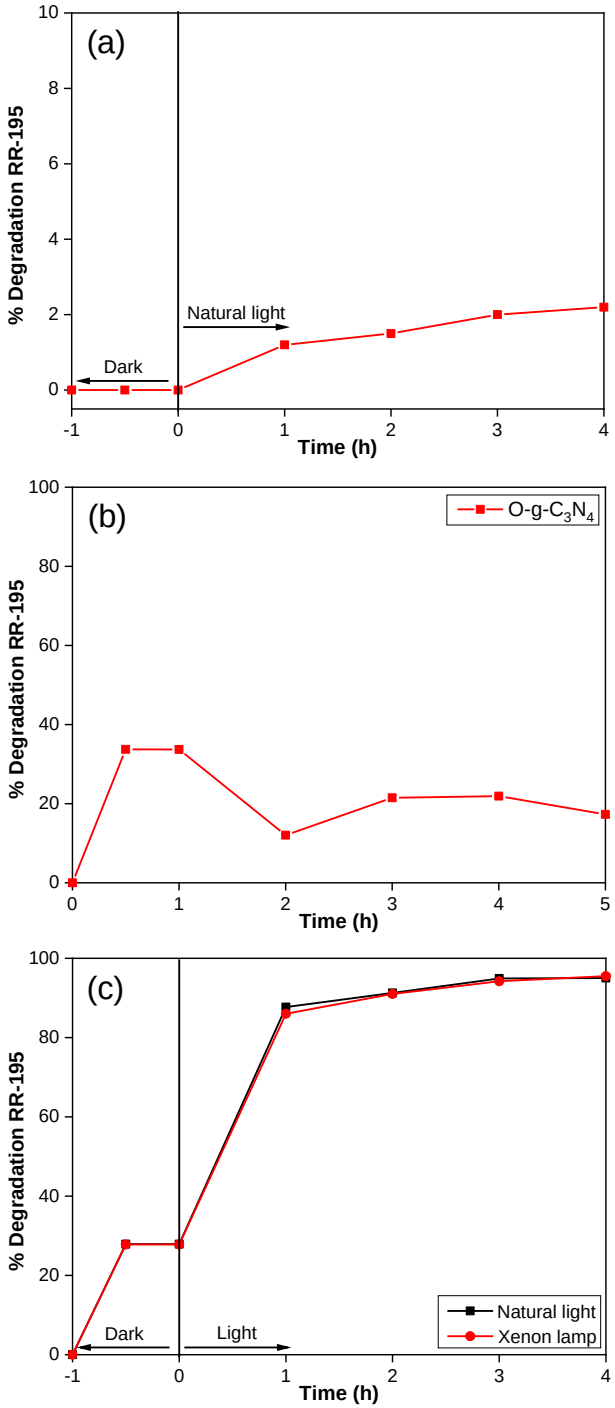

Figure S4. Photodegradation of RR 195 (a) without catalysts, (b) using O-g-C_3N_4 in the dark and (c) using O-g-C_3N_4 under natural sunlight and a xenon lamp 500 W

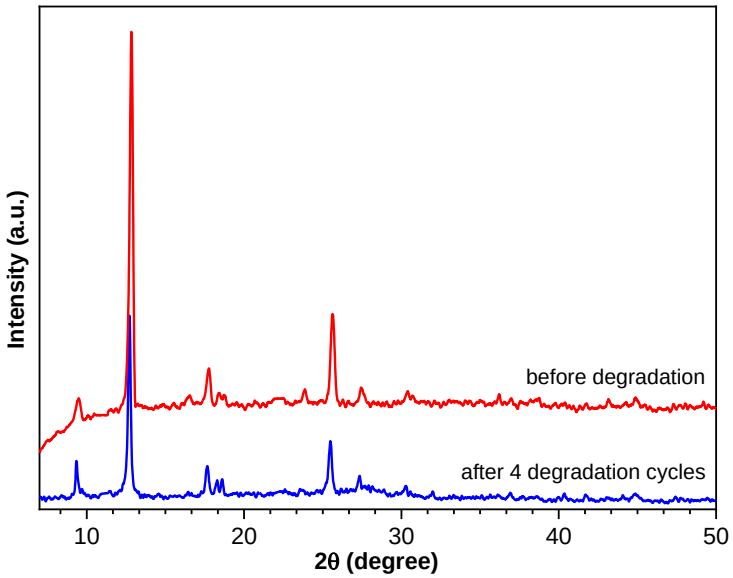

Figure S5. PXRD patterns of O-g-C_3N_4/MIL-53(Fe) before and after 4 degradation cycles

Table S3. Performance of O-g-C_3N_4/MIL-53(Fe) against other materials in photodegradation of azo anionic dyes (RR 195 and RY 145)

Azo Anionic dyes	**Samples**	**Concentration ($m_{catalyst}$/ C_{dyes})**	**Conversion (%)**	**References**
RR 195 and RY 145	O-g-C_3N_4/MIL-53(Fe)	50 mg/50 ppm	95.0 (RR 195); 99.0 (RY 145)	This study
RR 195	Titanium oxide (PK-10 and PK-180)	40 mg/50 ppm	99.0 (PK-10); 60.0 (PK-180)	Lambropoulou *et al.*[4]
	O-g-C_3N_4/H-ZSM-5	50 mg/50 ppm	96.6	Pham *et al.*[5]
	C-TiO_2 doped cellulose acetate	0.25 g/20 ppm	95.3	Pham *et al.*[6]
	Fe-ZSM-5@TiO_2	40 mg/50 ppm	98.0	Bahramifar *et al.*[7]
	ZnO/guar gum	25 mg/10 ppm	80.0	Allam *et al.*[8]
RR 145	$(Co, Ni)_3O_4/Al_2O_3$	0.1 g/50 ppm	80.0	Mohammad *et al.*[9]
	Fe-BTC/GO	30 mg/100 ppm	98.2	Vu *et al.*[10]
	Al_2O_3/ZrO_2	0.04 g/ 20 ppm	94.6	Yaghoubi *et al.*[11]

References

1 P. Kubelka and F. Munk, *Zeitschrift für Tech. Phys.*, 1931, **12**, 593–601.

2 Y. Jiang, P. Liu, Y. C. Chen, Z. Zhou, H. Yang, Y. Hong, F. Li, L. Ni, Y. Yan and D. H. Gregory, *Appl. Surf. Sci.*, 2017, **391**, 392–403.

3 J. G. Ibanez, M. Hernandez-Esparza, C. Doria-Serrano, A. Fregoso-Infante, M. M. Singh, J. G. Ibanez, M. Hernandez-Esparza, C. Doria-Serrano, A. Fregoso-Infante and M. M. Singh, in *Environmental Chemistry*, Springer New York, 2008, pp. 70–78.

4 B. Chládková, E. Evgenidou, L. Kvítek, A. Panáček, R. Zbořil, P. Kovář and D. Lambropoulou, *Environ. Sci. Pollut. Res.*, 2015, **22**, 16514–16524.

5 X. N. Pham, H. T. Nguyen, T. N. Pham, T. T. B. Nguyen, M. B. Nguyen, V. T. T. Tran and H. V. Doan, *J. Taiwan Inst. Chem. Eng.*, 2020, **114**, 91–102.

6 X. N. Pham, D. T. Pham, H. S. Ngo, M. B. Nguyen and H. V. Doan, *Chem. Eng. Commun.*, 2020, 1–14.

7 N. Aghajari, Z. Ghasemi, H. Younesi and N. Bahramifar, *J. Environ. Heal. Sci. Eng.*, 2019, **17**, 219–232.

8 M. Y. Rezk, M. Zeitoun, A. N. El-Shazly, M. M. Omar and N. K. Allam, *J. Hazard. Mater.*, 2019, **378**, 120679.

9 E. J. Mohammad, A. J. Lafta and S. H. Kahdim, *Polish J. Chem. Technol.*, 2016, **18**, 1–9.

10 H. T. Vu, M. B. Nguyen, T. M. Vu, · Giang, H. Le, T. T. T. Pham, T. Duy Nguyen and T. A. Vu, *Top. Catal.*, 1234, **63**, 1046–1055.

11 A. Yaghoubi, A. Ramazani and S. Taghavi Fardood, *ChemistrySelect*, 2020, **5**, 9966–9973.